Understanding Tornadic Wind Effects on Manufactured or Mobile Homes through High-fidelity CFD Simulations

Yi Zhao[a], Guirong Yan[b], Jiamin Dang[c], John W. van de Lindt[d], Ji Yun Lee[e], Daphne S. LaDue[f], and Cassandra A. Shivers-Williams[g,h,1]

[a] Missouri University of Science and Technology, Rolla, Missouri, US, yzvxd@mst.edu
[b] Missouri University of Science and Technology, Rolla, Missouri, US, yang@mst.edu
[c] Missouri University of Science and Technology, Rolla, Missouri, US, jdtbk@mst.edu
[d] Colorado State University, Fort Collins, CO, US, John.van_de_Lindt@colostate.edu
[e] Washington State University, Pullman, WA 99164, jiyun.lee@wsu.edu
[f] Center for Analysis and Prediction of Storms, Norman, OK, US, dzaras@ou.edu
[g] Cooperative Institute for Severe and High-Impact Weather Research and Operations, Norman, OK, US, cassandra.a.shivers@noaa.gov
[h] National Severe Storms Laboratory, National Oceanic and Atmospheric Administration, Norman, OK, US, cassandra.a.shivers@noaa.gov
[1] now at: Weather Program Office, National Oceanic and Atmospheric Administration, Silver Spring, MD, US, cassandra.a.shivers@noaa.gov

Abstract

Tornado fatality rates in the Southeastern United States are higher than those in Tornado Alley, despite Tornado Alley having a higher frequency of tornadoes. A major contributing factor is the large number of mobile and manufactured homes (MMHs) in the Southeastern states. Forensic engineering assessments of tornado damage have consistently shown that inadequate anchoring of MMHs or the absence of proper anchoring has been the primary cause of structural failure. To properly design an MMH anchorage system to resist tornadic winds, it is imperative to have accurate knowledge of the tornadic wind effects on the MMH systems. In this study, tornado-MMH interactions are investigated using high-fidelity numerical simulations. The pressure distribution on the MMH surface and the total forces/moments on the entire MMH induced by tornadic winds are obtained. In addition, simulations are conducted to reveal (1) the difference in tornadic wind effects between an MMH and its associated permanent home (home with classical on-site construction), and (2) the difference in wind effects between tornadic winds and the equivalent straight-line winds. The latter of these comparisons is intended to provide information on the unconservative use of straight-line wind loading for MMHs. The simulation results (peak wind pressure and total forces/moments on the MMH) are compared between the tornadic wind field and straight-line wind field. The comparison indicates that the results caused by the tornado are higher. Under a tornadic wind field, compared to the permanent home (PH), the peak pressure and horizontal forces on the MMH are smaller because of the existence of open space under the MMH. Although the research findings here demonstrate the limitation of the HUD code for MMHs, a great number of simulation cases with the related uncertainties involved will be needed to be run to improve the HUD code.

Keywords: Manufactured or Mobile Home, Tornado, Anchorage System, Computational Fluid Dynamics, Tornado Wind Effects

1. Introduction

In recent years, tornadoes have caused $10B in property losses annually (NWS 2018), although the potential is much higher. In the 2011 tornado outbreak, for example, tornado-induced property loss exceeded $20B, and 550 people were killed (FEMA 2012; Lott et al. 2012); the Joplin tornado alone resulted in $2.8B in direct losses (NIST, 2014). On average, the tornado fatality rate is the highest in the Southeast (SE) US, due to the high percentage of mobile and manufactured homes (MMHs) in the building stock (Strader et al. 2019). Fatalities are 15–20 times greater in an MMH than in a permanent home (PH; Sutter and Simmons 2010), with statistics for the past eight years (2011-2019) showing 20–68% of fatalities in MMHs during tornadoes (NWS 2019). Even though many counties in Alabama have community tornado shelters for MMH residents, those shelters can only house 2–17% of residents (LaDue 2019), which is a small portion of the individuals living in the 13% of housing stock that is MMHs (U.S. Census Bureau 2019).

During 21-22 January 2017 Southeast tornado outbreak, almost all deaths were reported in MMH (Strader and Ashley 2018). Figure 1a) illustrates a MMH rolled from its foundation and destroyed by the Washington County Tornado #1, which was classified as an EF1 tornado (NOAA 2023). Figure 1b) shows a destroyed MMH resulting from an EF1 tornado in 2017 (NOAA 2023). This particular MMH was flipped over by the tornado and then destroyed. Despite the relatively low intensity of these tornadoes, they still caused significant and extensive damage to MMHs. Figure 1c) shows the aftermath of an EF2 tornado in 2017 tornado outbreak, where a MMH in Wilcox County was completely destroyed. The entire MMH collapsed and were blown into pieces by the wind of this EF2 tornado. These instances serve as compelling evidence for the vulnerability of MMHs when being confronted by tornadoes, even with a low intensity.

a) b) c)

Fig. 1 Damages on MMHs due to tornado attack: a) A rolled and destroyed MMH by Washington County Tornado #1 (NOAA 2023); b) A flipped and destroyed MMH by Washington County Tornado #2 (NOAA 2023); c) A Destroyed MMH by Wilcox Tornado (NOAA 2023).

Beginning on 15 June 1976, the Department of Housing and Urban Development (HUD) began to regulate the construction of all MMHs built in the US through the enforcement of Manufactured Home Construction and Safety Standards (HUD codes). However, state, local, and regional building codes (e.g., International Building Code, ASCE 7, ACI 318, etc.) are not mandatory, and structural approval by a local inspector is generally not required. In addition, the current MMH design uses wind load modification from ASCE 7-88 (released in 1991), which is determined using straight-line synoptic winds, not based on tornadic winds. Thus, it is not surprising to see many of these MMH homes failed during tornadoes.

In fact, inadequate anchorage to the ground is consistently shown as the primary cause of MMHs failure in post-tornado forensic engineering assessments (Roueche et al. 2019). Regardless of anchorage, though, Roueche's findings indicate that MMH anchoring systems may not have the capacity to withstand tornadoes. In order to determine a proper design for the anchorage system and reduce fatalities during tornadoes, it is critical to fully understand the wind effects induced by tornadoes on MMHs. Previous studies have simulated tornadoes in laboratory tornado simulators or used CFD simulations to study tornadic wind effects on PHs (Selvam and Millett 2003; Sengupta et al. 2008; Mishra et al. 2008; Haan et al. 2010; Hu et al. 2011; Sabareesh et al. 2012; Refan 2014; Razavi and Sarkar 2018). Mishra et al. (2008) investigated the pressure distribution caused by a stationary tornado on the walls and roofs of a cubic structure. Their results indicated that the pressure distribution induced by a tornado differs significantly from that induced by ABL winds in terms of both magnitude and the locations of positive and negative pressure values. Haan et al. (2010) conducted a study on the tornado-induced loads on a low-rise building with a gable roof with a pitch of 35° and a plan aspect ratio of 1. They found that horizontal and uplift loads were 50% and 200-300% larger compared to the loading calculated based on the wind pressure equation provided in ASCE7-5, respectively. Sabareesh et al. (2012) found that the distance between tornado and building significantly affected the magnitude of the tornado induced loads on a cubic building. Razavi and Sarkar (2018) examined the effects of swirl ratio, translation speed, and the distance and orientation of a building in relation to the tornado-track center. They found that the maximum loads occurred at locations that were not at the immediate center of the tornado; significantly larger peak load coefficients were obtained under the tornado with lower swirl ratio; peak roof uplift increased with increase in translation speed when the building was on the tornado path. However, little research has investigated tornadic wind effects on MMHs. To bridge this research gap, the objective of this study is to investigate the wind effects on MMHs induced by tornadoes and provide guidance for future wind resistance design for MMHs.

The remainder of the paper is arranged as follows. In Section 2, the simulated tornado is introduced, and simulation setup and simulated cases, as well as grid independence study, are described; in Section 3, tornadic wind effects on an MMH are extracted, in terms of force coefficients, moment coefficients, and pressure on MMH's surface. The pressure/velocity contour and streamlines in the wind field surrounding the MMH, which is associated with critical locations, are presented to explain the impact of the tornado on the MMH. In Section 4, CFD simulation is run to study the interaction between the simulated tornado and a permanent home (PH) associated with this MMH, to reveal the difference in tornadic wind effects between an MMH and a PH. In Section 5, an equivalent straight-line wind field is simulated, in order to simulate its action on the MMH. This reveals the difference in wind effects on the MMH between tornadic winds and the equivalent straight-line winds, as the current wind design of MMHs is still based on straight-line winds. Finally, conclusions are drawn, and future works are described.

2. Simulation Setup

2.1 Simulated tornado

In order to investigate the wind effects on MMHs induced by tornadoes, the data of the Spencer, South Dakota (SD) Tornado of 30 May 1998 (hereafter, referred to as

“Spencer Tornado”) is used to generate a tornadic wind field. The Spencer Tornado spawned in the west of Spencer, SD, and tore through the heart of the town on the night of May 30, 1998. It was rated as an F4 tornado and had a double-celled, single-vortex flow structure during most periods of its lifecycle. The radar-measured velocity data of Spencer Tornado were collected by Doppler on Wheels radar (Wurman, 2005; Kosiba and Wurman, 2010) and the radar-measured data at 0134:23 UTC as shown in Fig. 2) were used to generate the tornadic wind field successfully (Zhao et al. 2021). In this study, Spencer Tornado is scaled down to an EF2 torando to examine the tornadic wind loads on the MMHs.

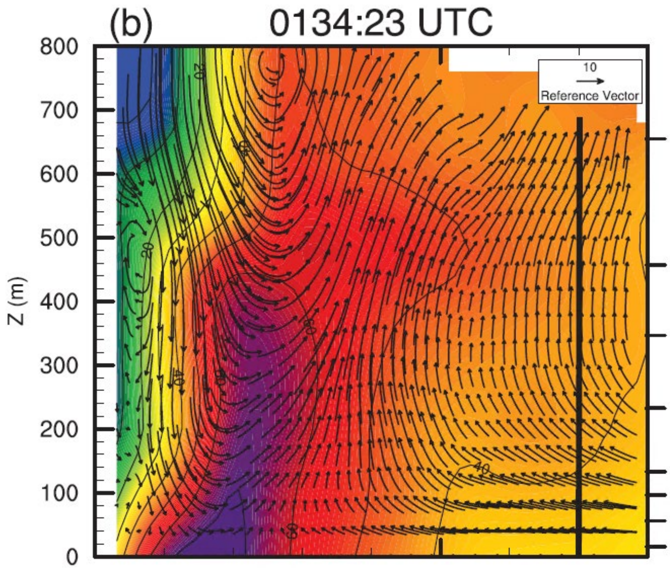

Fig. 2 Velocity field of Spencer Tornado on a vertical plane (Kosiba and Wurman, 2010)

To simulate the swirling wind flow, a cylindrical computational domain is applied, as shown in Fig. 3a). The radius of the computational domain is 800 m, and the total height is 1100 m. The inflow is set up as the velocity inlet on the side; the outlet is set up as the pressure outlet on the top. Within the United States, MMHs are categorized into two primary sizes: single-wide and double-wide. Single-wide measures about 14-18 ft in width and 70 ft in length. These units can be transported to their intended locations as a single unified structure. On the other hand, double-wide is 20 feet or wider and have a similar length as the single-wide, which are transported to the construction location in two separate units. In this study, a single-wide MMH structure is placed inside the computational domain and set up as a rigid body, as shown in Fig. 3a). As shown in Fig. 3c), the length and width of the building are 21.34 m (70 ft) and 4.27 m (14 ft), respectively. The eave height is 2.74 m (9 ft) and the roof ridge height is 4.11 m (13.5 ft). In accordance with the HUD code, MMHs are required to maintain a minimum clearance of 12 inches between the lowest member of the main frame and the ground. It is common for modern MMHs to have this clearance exceeding 25 inches. For better appearance, skirting is often used, which can also protect the in-ground anchoring system and underbody frame to a certain degree. However, it is important to note that skirting does not serve as a structural component and is not firmly connected to the MMH. Consequently, it is susceptible to being blown away or damaged easily during tornado events, even before the vortex arrives. Moreover, many older MMHs, particularly those found in mobile home parks, lack skirting altogether. From these aspects, the study only explored the scenarios assuming the absence of skirting. A open space with a height of 1.016 m (40 in) is set and it is considered as a fluid domain that allows the air to flow freely. The orientation of this building with respect to the *x* direction is 0 degrees, which means the long side of the building is parallel to the *x* direction, as shown in Fig. 3b). In this way, the longer dimension of the MMH is perpendicular to the tangential wind direction, which is the dominated velocity component at the core radius of tornado. This building orientation might be the worst wind loading scenario, which is consistent with the fact that MMHs were rolled/flipped when the tornado approaches to the MMHs in the direction perpendicular to their longer sides in previous tornado incidents, as shown in Fig. 1a) and Fig. 1b). A transient, incompressible CFD simulation is conducted.

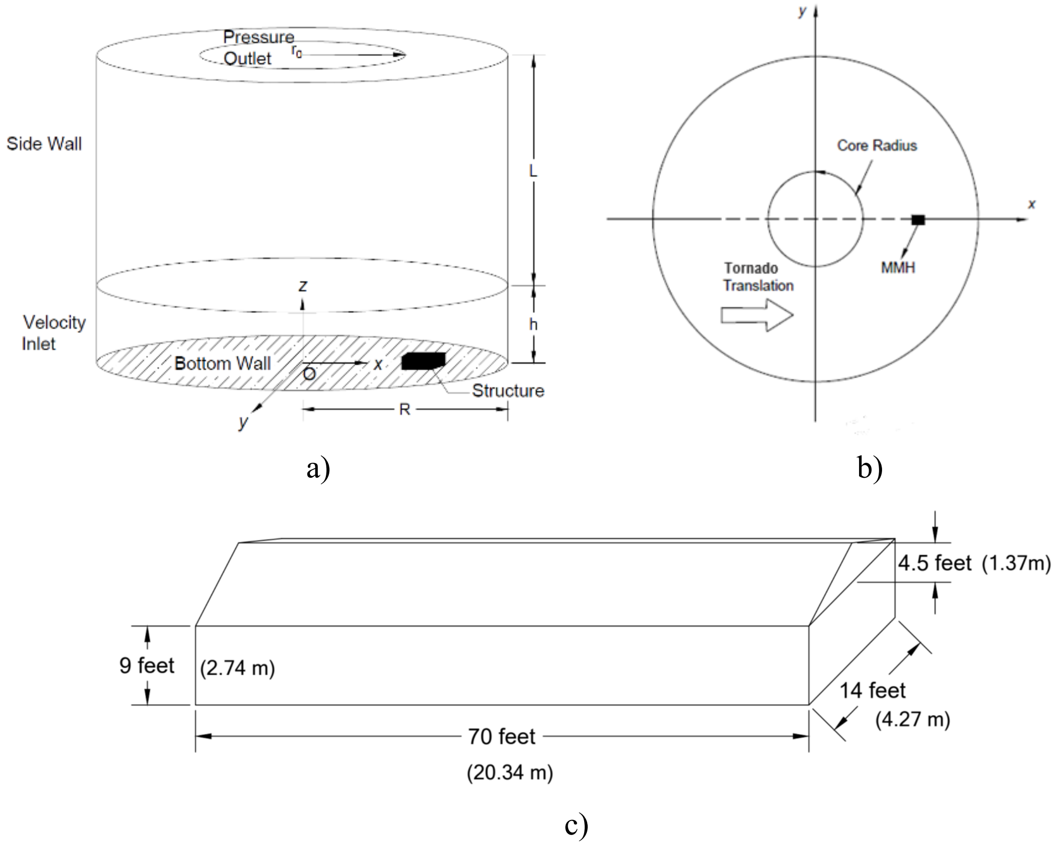

Fig. 3 Computational domain, tornado translation path, and an MMH structure of interest. a) Computational domain; b) Tornado translation path; c) Dimensions of a single-wide MMH structure.

To simulate that a tornado translates and passes by the MMH, a relative motion is established by moving the MMH in the opposite direction, at the same speed as tornado translation, as shown in Fig. 3b). To be specific, the entire computational domain is divided into several zones, with the zone including the MMH as “a rigid body zone”. The translation of MMH is achieved by applying a constant moving speed on the “rigid body zone” (to the left in this case) and applying the layering dynamic mesh technique on the two zones before and after the “rigid body zone” along the long strip, which is treated as deforming zones, as shown in Fig. 4. In this way, the “rigid body zone” with the MMH translates through the two deforming zones and the deforming zones are adjusted automatically. In the remaining zones on the bottom wall, the bottom walls are set up as “moving wall” with the same speed in the same direction as the tornado translation. The upper zone is set up as a stationary domain (i.e., no mesh would be changed or updated). In this study, the translation speed is selected as 15 m/s, which falls in the range of general tornado's translation speeds (10m/s to 30 m/s). First, the simulation is run for 500 s with the MMH staying at the original place (stationary stage) to simulate the action of a stationary tornadic wind field on the MMH. Then, the MMH is moved to pass through the tornado (translating stage). The center of the MMH is initially set up at x = 500 m in the stationary stage and then it translates along the negative x direction in the translating stage. The mesh of the computational domain is developed in Pointwise v18.4 and the hybrid mesh strategy is adopted. The structured hexahedral grid is adopted for almost all zones except the "rigid body zone", as shown in Fig. 4b), where the unstructured mesh is applied. In addition, for the "rigid body zone", the t-rex mesh technique is performed around the building and above the ground.

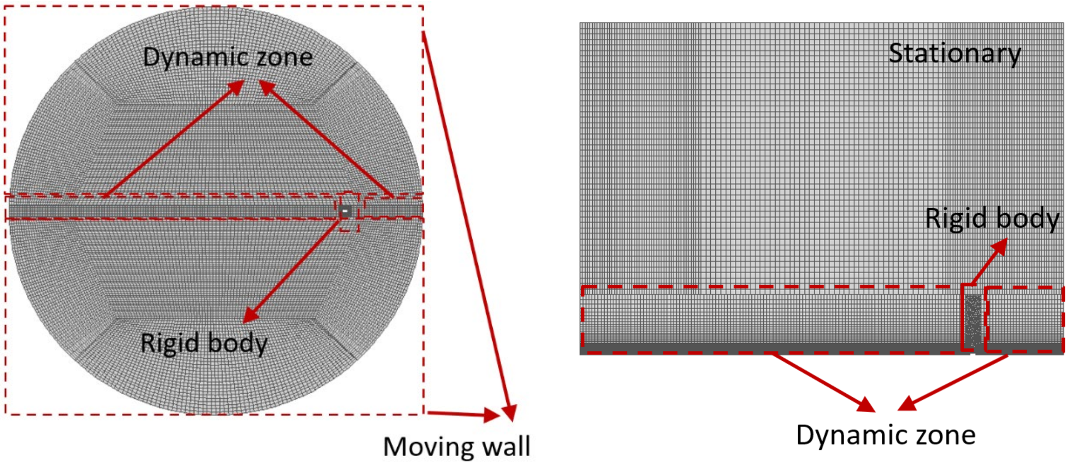

a) b)

Fig. 4 Computational domain mesh and simulation setup for tornado translation. a) Horizontal view; b) Vertical view.

It is well-known that it is critical to properly deal with turbulence modeling in CFD simulations. Reynolds-averaged Navier-Stokes (RANS), Large Eddy Simulation (LES), Wall-Modeled LES (WMLES), and Detached Eddy Simulation (DES) are all CFD methods used for simulating turbulent flows. RANS solves the time-averaged Navier-Stokes equations and the computation cost is not expensive, but can only provide the statistical information about the turbulent flow field. LES is a technique that resolves the large-scale turbulent structures while modeling the smaller, unresolved scales and it is particularly suitable for capturing the dynamic features of turbulence, such as vortices and coherent structures. WMLES is an approach that combines LES with a wall model (RANS) to handle the near-wall region of the flow more efficiently. DES is a hybrid approach that combines the RANS and LES methodologies to capture both the attached and detached turbulent boundary layer regions. It applies LES in regions of the flow where the turbulence is strong and unsteady, while using a RANS model in regions where the turbulence is weak and steady. Despite different ways to deal with turbulence setup in CFD simulations, some previous tornado simulation research did successfully obtain solid results by using Large Eddy Simulation (LES), such as tornado wind filed simulation (Ishihara et al. 2011; Natarajan and Hangan 2012), and tornado-building interaction simulation (Sengupta et al. 2008; Liu et al. 2018). Therefore, LES with a WALE (wall-adapting local eddy-viscosity constant, Cwale=0.325) subgrid model is directly applied to conduct the CFD simulation in this study (Nicoud and Ducros, 1999). The segregated implicit solver is used to solve the transient, incompressible flow with a Semi-Implicit Method for Pressure Linked Equation-Consistent (SIMPLEC) method for Pressure-velocity Coupling, as the SIMPLEC scheme usually has a better convergence than Pressure–Implicit with Splitting of Operators (PISO) (Van Doormaal and Raithby, 1984; Hangan and Kim 2008). In addition, the simulation applies the Least Squares Cell Based scheme for Gradient, which is used to discretize the convection and diffusion terms in the flow conservation equations, the second-order discretization scheme for the pressure equation, and the bounded central differencing scheme for momentum convection-diffusion equation (Anderson and Bonhaus, 1994; Barth and Jespersen, 1989; Leonard, 1991). The bounded second-order implicit method with a time step of $\Delta t = 0.02s$ is used for time discretization for the stationary stage and then the second-order implicit method is used for the translating stage. The density of 1.225 kg/m^3, the temperature of 288.15 K, and the dynamic viscosity of 1.789×10-5 kg/(s*m) are adopted at the inlet and outlet and considered as the initial condition for the entire computational domain. In this study, the maximum Courant Number in the simulation is 0.7061 to ensure that the stability condition is met. The pressure of 95000 N/m^2 is assumed as the inner pressure of the MMH, which is considered to be constant during the entire calculation. A pressure deficit curve is applied at pressure-outlet as the pressure boundary condition, as shown in Eq. (1).

$$P = \begin{cases} -9000\ Pa, r \leq 40\ m \\ -4047e^{-0.002972*r} - 5393e^{0.0001537*r}, r > 40\ m \end{cases} \quad (1)$$

where P is the static pressure at the radius of r.

2.2 Simulated cases

In order to characterize tornadic wind effects on MMHs, three cases are simulated in this study, as listed in Table 1. Case 1 simulates an MMH with no skirting between the first-floor elevation and the ground; Case 2 simulates an associated permanent home (PH, has the same geometry but the open space in Case 1 is closed and considered as the structural component) that experiences the same tornadic winds as in Case 1; and Case 3, the MMH (same as in Case 1) is placed in an equivalent straight-line wind field (adopting the horizontal wind speed at the height of 10 m in the tornadic wind as the reference wind speed in the straight-line wind field) to investigate the difference in wind effects on the MMH between tornadic winds and straight-line winds, as the current wind design of MMHs is based on straight-line winds. For Case 2, the translation of PH is set up in the same way as in Case 1.

Table 1. Simulated cases to investigate wind effects on MMHs.

Case #	Simulation Description
Case 1	MMH with no skirting is placed in a tornadic wind field
Case 2	The associated PH is placed in the same tornadic wind field
Case 3	MMH with no skirting is placed in the equivalent straight-line wind field

2.3 Independence study of grid

To examine the grid independence, three simulations are run. In the first simulation, the number of cells is about 3 million (coarse mesh, thickness of the first layer on structure surface and ground = 0.005 m); In the second simulation, the number of cells is about 5 million (thickness of the first layer on structure surface and ground = 0.003 m); In the third simulation, the number of cells is about 8 million (thickness of the first layer on structure surface and ground = 0.002 m). After the simulations become stable, the space-averaged tangential velocity profile at the height of 80 m is extracted from each simulation and is presented in Fig. 5. The three profiles follow the same trend, and the differences in the maximum tangential velocity are 0.91% and 1.62%, respectively, when taking “Coarse mesh” as the baseline, while all the three simulations achieve the same core radius. To balance the computational cost and computational accuracy, the “Coarse mesh” is adopted for the following simulations. The mesh produced by Pointwise was evaluated by the mesh quality evaluation tool in FLUENT. The mesh has a minimum orthogonal quality of 0.028 and a maximum aspect ratio of 34.6, which fall in the range of suggested values by FLUENT (> 0.02 and <35, respectively). Based on the previous simulation (Zhao et al. 2021) and checking through animation, at 450s, the formation of the tornado vortex is observed. By comparing the tangential velocity profiles at 500 s and 450 s as shown in Fig. 5d), it is found that the maximum difference in the tangential velocity profile is less than 5%, which means the formed tornado vortex becomes steady. Therefore, the duration of the stationary stage is set as 500 s.

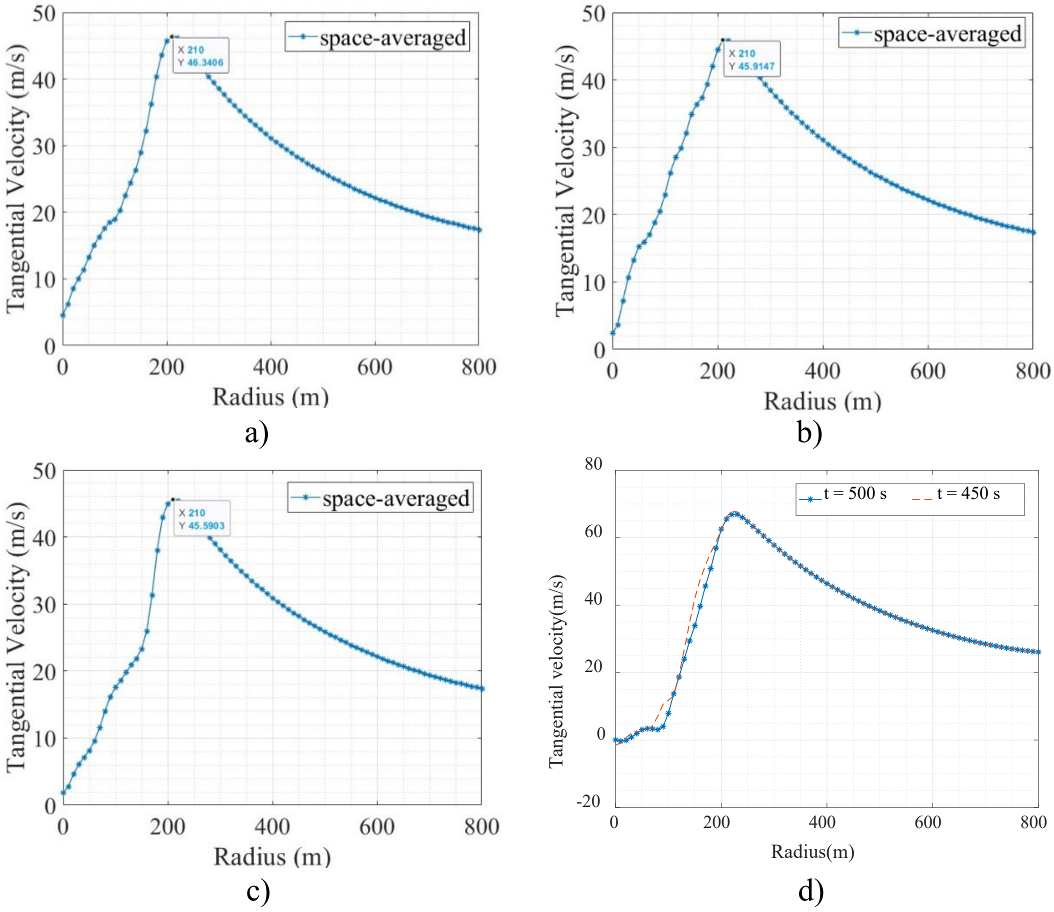

Fig. 5 Tangential velocity profiles extracted from the simulations with different cell numbers for independence study of grid and simulation duration. a) Coarse mesh; b) Fine mesh; c) Finer mesh; d) t =450 s & 500 s.

3. Simulation Results and Discussion

3.1 Simulated tornadic wind field

To demonstrate the flow structure of the simulated tornadic wind field, the streamlines and contour of pressure on the horizontal plane at z = 80 m and on a vertical plane through tornado center (at x = 0 m) are extracted and presented in Fig. 6. In Fig. 6a), only one large vortex is observed in the central area, verifying that the tornado possesses a single vortex. The static pressure at the outer region of the tornado is around -6300

N/m^2, and it gradually decreases along the radius to -9300 N/m^2 at the tornado center. In Fig. 6b), it is observed that a downdraft is formed at the center and touches the ground, while an updraft is formed in the surrounding area, forming two different circular regions, which indicates a double-celled flow structure. Based on the above observations, the simulated tornado is a double-celled single-vortex tornado. However, it should be noted that as the MMH's height is relatively small, close to the ground, the wind field around the MMH may be more turbulent than that at higher elevations, with a more complicated flow structure.

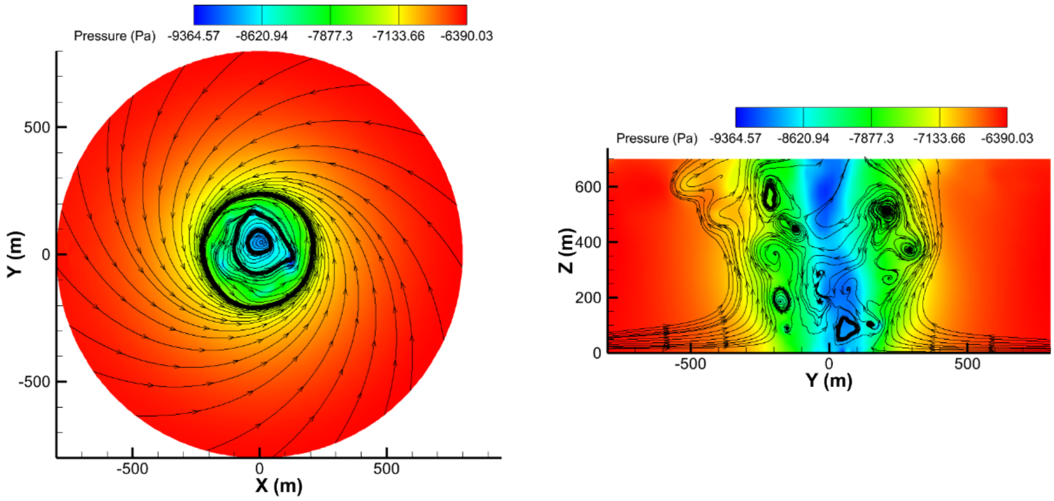

a) b)

Fig. 6 Streamlines and contour of pressure in wind field. a) On a horizontal plane; b) On a vertical plane.

3.2 Tornadic Wind Effects on MMH (Case 1)

3.2.1 Force and Moment Coefficients

To find the total actions of the tornado on the MMH, the instantaneous force/moment coefficients are obtained when the MMH moves from one side of the tornado to the other side. The total forces and moments exerted on the entire MMH are calculated by integrating the static pressure acting on the surface of the building. Then, the force coefficients along the *x*, *y,* and *z* axes and the moment coefficients about the three axes are calculated as follows:

$$CF_x = \frac{F_x}{\frac{1}{2}\rho V^2 S}, CM_x = \frac{M_x}{\frac{1}{2}\rho V^2 Sh} \tag{2}$$

$$CF_y = \frac{F_y}{\frac{1}{2}\rho V^2 S}, CM_y = \frac{M_y}{\frac{1}{2}\rho V^2 Sh} \tag{3}$$

$$CF_z = \frac{F_z}{\frac{1}{2}\rho V^2 S}, CM_z = \frac{M_z}{\frac{1}{2}\rho V^2 Sb} \tag{4}$$

where F_{sub} is the total force along each axis, M_{sub} is the total moment about each axis through the building center, ρ is the air density, V is the maximum space-averaged resultant horizontal wind velocity at the height of 10 m and at the core radius of the tornado (determined when no buildings are present in the tornadic wind field), S is the projected area on the longer side, h is the height of roof ridge, and b is the longer dimension of the MMH.

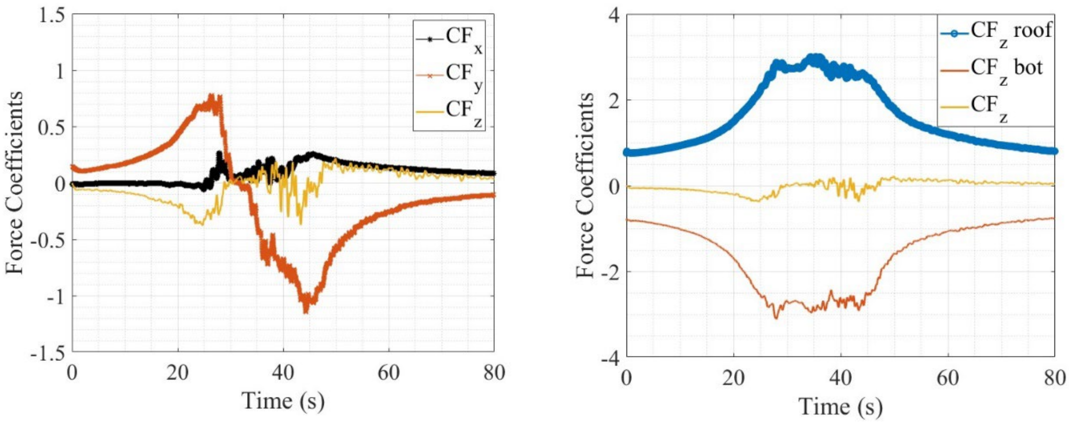

a) b)

Fig. 7 Force coefficients when the MMH moves from one side of the tornado to the other side (Case 1). a) *CF* in the *x, y, z* directions; b) *CF* in the *z* direction.

Figure 7 presents the instantenous coefficients of the forces acting on the MMH in Case 1. CF_x and CF_y are the force coefficients along the *x* and *y* directions (horizontal directions), while CF_z represents the coefficient of the total force along the *z* direction (vertical direction) acting on the entire building (the sum of the force acting on the top of the roof and the force acting under the floor bottom). The horizontal axis of Fig. 7 represents the duration of tornado translation (i.e., the period during the MMH moves from one side of the tornado to the other side in the simulation). As shown in Fig. 7a), as the MMH moves to the left (towards the tornado center), the three force coefficients gradually increase and reach their respective first peaks simultaneously at around t = 25 s, when the MMH is very close to the core radius. After the building passes the core radius and approaches the tornado center, the absolute values of all three force coefficients decrease gradually with the decreasing relative distance to the tornado center. The building arrives at the tornado center at t = 33.33 s. After the building passes the tornado center, these values switch to increase with increasing relative distance and reach their peaks when the MMH reaches the core radius on the other side of the tornado (at around t = 42 s). Among all the three force coefficients, CF_z is not dominant, which is a major difference compared to that observed on a permanent house, as shall be elaborated in Section 4; In fact, CF_y is much greater than CF_x and CF_z. In addition, the sign of CF_y changes from positive (pointing to the positive *y* direction) to negative (pointing to the negative *y* direction) when the building passes the tornado center from one side of the tornado to the other side, which are consistent with the direction change of the tangential velocity component (a counterclockwise vortex in the North Hemisphere).

From the above results, CF_y is the dominant force coefficient, while CF_z is much smaller. Does this mean that the uplift force (the force in the vertical direction) is too small to damage the MMH? To answer this question, CF_z acting on the roof (designated as "CF_z roof") and CF_z acting under the floor bottom (designated as "CF_z bot") are extracted and presented in Fig. 7b), along with CF_z (the sum of the CF_z roof and *CFz* bot). Compared to CF_z, CF_z roof and *CFz* bot present much larger peak values (3.1 and -3.2, respectively). During the entire period, CF_z roof and CF_z bot are applied in the opposite direction, while the magnitudes are very similar, which indicates that the pressure on the surface is mainly caused by the atmospheric pressure in the tornadic wind field (the contribution from aerodynamic pressure is minimal). During the entire period of tornado loading, CF_z roof remains positive which is an upward force to lift the roof up, while CF_z bot remains negative, which is a downward force to pull the floor bottom down. The upward force acting on the roof and the downward force acting on the floor bottom of MMH are associated with negative pressure on the two surfaces. The negative pressure here is attributed from the large atmospheric pressure drop at tornado center and the aerodynamic pressure due to the flow acceleration when the flow passes above and underneath the MMH, although the impact of aerodynamics of the structure are minimal. In summary, although the total force along the *z* direction acting on the entire MMH is not large, it does not mean that the MMH is not damaged by the force in the vertical direction. In fact, the structural body of the MMH experiences one pair of large tensile force along the vertical direction for a certain period (when tornado core passes the building); The significant uplift force on the roof and the downward force on the floor bottom may cause severe damage to the roof, the floor bottom, and roof-wall and floor-wall connections. The damage to the roof and roof-wall connection can result in some openings on the roof of MMH, which may further damage properties inside the building. This finding is consistent with the fact that the damage to roof is the most common failure mode for MMHs during tornado incidents.

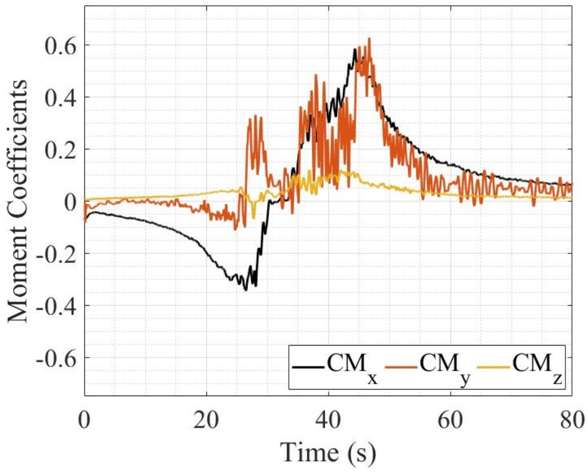

Fig. 8 Moment coefficients when the MMH moves from one side of the tornado to the other side

As shown in Fig. 8, when the building moves from the right side of the tornado to the left side, the changing trend of the magnitudes of moment coefficients are similar to the force coefficients. During the tornado attack, the sign of CM_y and CM_x changes from negative to positive when the building passes the tornado center, which indicates that MMH is always bent toward tornado center and is bent toward the tangential direction. It is worth noting that CM_z is always positive when MMH is outside the core radius but fluctuates around 0 when MMH is inside the tornado core. This indicates that MMH is rotated counterclockwise, which is the same as the rotation of the tornado (counterclockwise). On the other hand, due to the low wind speed and high turbulence of the flow inside the tornado core, MMH may be rotated to different direction when it is in the tornado core region. The fact that all force and moment coefficients present peak values near the core radius demonstrate that MMH is likely to experience more severe damage when it is around the core radius.

3.2.2 Pressure Distribution and Streamlines in Wind Field around the MMH

Figure 9 presents the contours for pressure, velocity, and streamlines on a vertical plane and a horizontal plane through the MMH when the MMH moves to the core radius for the first time. In Fig. 9a), it is observed that partial incoming air flows the open space under the MMH, while the other parts of incoming air flow over the roof and on the two sides of the building. The stagnation point is nearly at the middle point of the windward wall and the maximum pressure is found at this stagnation point, which is around -6300 Pa. The negative value (-6300 Pa) is due to the fact that the atmospheric pressure in the entire tornadic wind field is lower than standard atmospheric pressure. Behind the MMH, a large turbulent area is formed near the leeward wall and negative pressure is present in this area, which is about -9400 Pa. The disturbed airflow area by the presence of the MMH (Wake Area) is above the open space below MMH and the maximum height of this area is a little higher than the MMH's ridge. In Fig. 9b), the speed of incoming air decreases due to the blockage of the MMH as it approaches the windward wall, and then it accelerates to flow over the MMH. The maximum velocity is found over the roof and in the open space below MMH, which is about 80 m/s. The wind speed in the Wake Area is lower than 2 m/s (near the leeward wall and leeward roof). On the horizontal plane, as shown in Fig. 9c) and Fig. 9d), winds acting on the MMH with an angle of 30 degree and accelerate to pass the two corners of the MMH. This results in high pressure on the windward wall (Wall AB) and low pressure on all other surfaces, as shown in Fig. 9e). It is noted that the maximum negative pressure occurs at the corner between the windward wall and roof (on the roof), the corner between windward wall and floor (on the floor) due to the fact that vortices are formed when air flows over these corners.

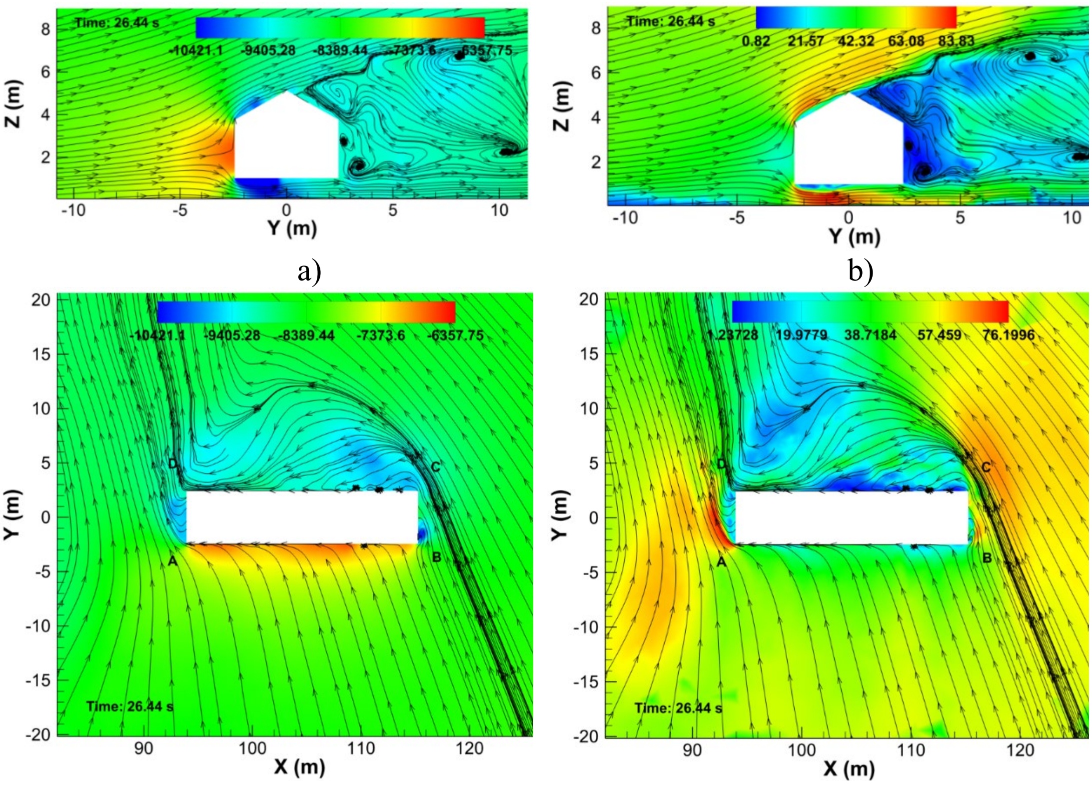

a) b) c) d)

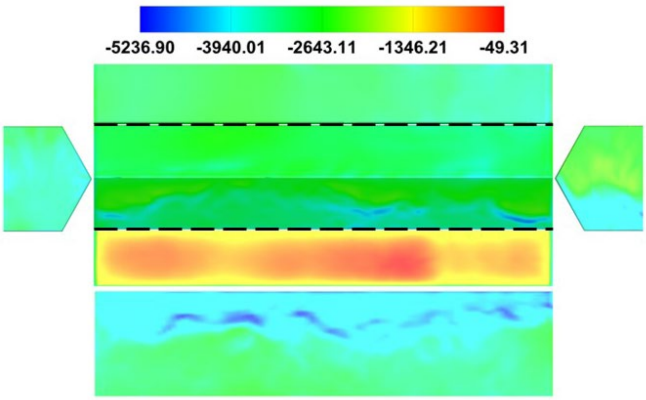

e)

Fig. 9 Contours for pressure, velocity and streamline when the MMH is near the core radius: a) Contour of pressure and streamline on the YZ plane through MMH; b) Contours for velocity magnitude and streamline on the YZ plane through MMH; c) Contours for pressure and streamline on the XY plane through MMH at the height of 3 m; d) Contours for velocity magnitude and streamline on the XY plane through MMH at the height of 3 m; e) Contours for pressure on MMH's surface.

Based on the Manufactured Home Construction and Safety Standards, for MMHs, for Wind Zone I, the main wind-force resisting component must be designed for horizontal wind pressure of not less than 15 psf (718 Pa) and a net uplift roof pressure of not less than 9 psf (431 Pa). For Wind Zones II and III, the design wind loads refer to ASCE 7-88, "Minimum Design Loads for Buildings and Other Structures". For a fifty-year mean recurrence interval, the design wind speeds of 100 mph and 110 mph are applied for Wind Zone II and for Wind Zone III, respectively. The associated design wind pressure can be calculated by the equation specified in ASCE7-88, as shown in Eqs. (5) & (6).

$$P = q * G_h * C_p - q_h(GC_{pi}) \tag{5}$$

$$q(q_h) = 0.00256 * K_z * (I * V)^2 \tag{6}$$

where P is the wind pressure (psf), $q(q_h)$ is velocity pressure, V is the wind speed, $I =$ 1.07 for areas 100 miles away from the coast and 1.11 for areas at the hurricane oceanline, $K_z = 0.8$, $G_h = 1.32$, $GC_{pi} = +/-0.25$, and C_p=0.8 (windward wall), -0.5(leeward wall), -0.7(side wall), -0.2(windward roof), -0.7(leeward roof).

For a MMH that is located in New Orleans near the hurricane oceanline, which in Wind Zone III (HUD), based on the equations above, the associated design wind pressure, force/moment coefficients are obtained, as listed in the Tables 2&3.

Table 2 Wind pressure based on ASCE 7-88 & ASCE 7-22.

	ASCE 7-88 (kPa)	ASCE 7-22 (kPa)	Simulation (kPa)
Windward wall	1.83	1.81	-1.34
Leeward wall	-1.28	-1.38	-2.64
Sidewall	-1.66	-1.68	-3.90
Windward roof	-0.72	-0.93	-5.20
Leeward roof	-1.66	-1.49	-3.82

Table 3 Force/moment coefficients based on ASCE 7-88 & ASCE 7-22.

	ASCE 7-88	ASCE 7-22	Simulation
CF_x	0	0	0.28

CF_y	1.07	0.83	1.16
CF_z	0.72	0.82	3.20
CM_x	0.37	0.25	0.59
CM_y	0	0	0.63
CM_z	0	0	0.15

For comparison, the design wind pressure based on the latest ASCE 7-22 "Minimum Design Loads for Buildings and Other Structures" is calculated and the related equations are listed in Eqs. (7) & (8). The associated design wind speed at the same location (New Orleans) is 138 mph.

$$P = q * K_d * G * C_p - q_i K_d (GC_{pi}) \quad (7)$$

$$q(q_h) = 0.00256 * K_z * K_{zt} * K_e * V^2 \quad (8)$$

where $K_d = 0.85$, $G = 0.85$, $K_z = 0.85$, $K_{zt} = 1$, $K_e = 1$, and $GC_{pi} = +/-0.55$ (partically enclosed building). The C_p values are the same as the ones used in Eq. (5). For the same MMH, the associated design wind pressure/force coefficients are also listed in the Tables 2 &3. In addition, it is worth to note that the added Chapter 32 Tornado loads in the ASCE 7-22 is not applicable as it is only for Risk Category III and IV buildings (MMH is rated as Risk Category II).

On the other hand, in the associated tornadic wind field, the obtained maximum wind pressure is -5237 Pa, which occurs on the roof; and the maximum force/moment coefficients are 1.16 (CF_y), 3.2 (CF_{z_roof}), and 0.59 (CM_x), respectively. By comparing the results from tornadic wind field with the results based on ASCE 7-88 in Tables 2&3, it shows that both wind pressure and forces on the MMH are more significant than the design wind load, especially on the roof. For the results based on ASCE 7-22 in Tables 2&3, the design wind pressure on leeward wall, sidewall, and windward roof as well as force coefficient along z-direction are amplified over ASCE 7-88. However, they are still much lower than the tornadic wind loads. In fact, the high wind pressure on the roof is consistent with the observation that the roof of MMHs is often found to be damaged. The difference of the results in Table 3 from those obtained in the tornadic winds is actually caused by the improper values of C_p. Currently, the C_p value specified in ASCE 7 is based on the assumption of straight-line winds (atmospheric boundary layer wind), not tornadic winds. In fact, the C_p values are completely different for each wall/roof under tornadic winds. In addition, the C_p value in ASCE was obtained based on the assumption that the structure of interest is built from the ground, with no "air gap" between the bottom of the building and the ground. In reality, for MMHs, there is an "air gap", which significantly changes the aerodynamics around the MMHs. This makes the C_p values different between the MMHs and regular civil structures.

4 Comparison of Tornadic Wind Effects between MMH and Permanent House (PH) (between Case 2 and Case 1)

Figure 10 presents the coefficients of the forces/moments acting on the associated PH (Case 2) under the same tornadic wind field as in Case 1. As shown in Fig. 10a), as the PH moves to the left (towards tornado center), CF_x, CF_y and CF_z gradually increase and reach the first peaks simultaneously at around t = 24 s. After the building passes the tornado center, CF_y and CF_z keep increasing with increasing relative distance and reach the maximum peaks when the PH reaches the core radius on the other side of the tornado (at around t = 45 s). Among all the three force coefficients, peak CF_z is dominant, which has also been observed in previous studies on a gable-roofed house (Haan et al., 2010).

This is a distinct difference in tornadic wind effects between an MMH and a PH. This is because CF_z in Case 2 only needs to account for the force acting on the roof since a PH sits on the ground, while CF_z in Case 1 accounts for the forces acting on both the roof and the floor bottom because of the open space between the MMH and the ground. In fact, CF_z in Case 2 is similar to CF_z roof in Case 1. Compared to Case 1, the CF_x and CF_y in Case 2 are about 1.33 times and 1.18 times of CF_x and CF_y in Case 1, respectively, which will be reasoned later. Figure 10b) shows the moment coefficients of PH and the peak values also occur near the core radius. To validate the CFD simulation results, the obtained force coefficients are compared from the those obtained from experimental testing (Haan et al., 2010). In their study, one-story gable roof building (91 mm (length) X 91 mm (width) X 36 mm (eave height)) was tested in the tornado simulator at Iowa State University. A total of five different tornado vortices were simulated to pass through the gable roof building and the range of force coefficients were reported as CF_y:1.2-1.8; CF_z: 2.2-3.8. The maximum values of CF_y (1.26) and CF_z (3.22) in numerical simulation of this present study do fall in the range of the experimental results, which further validates the numerical simulations in this study.

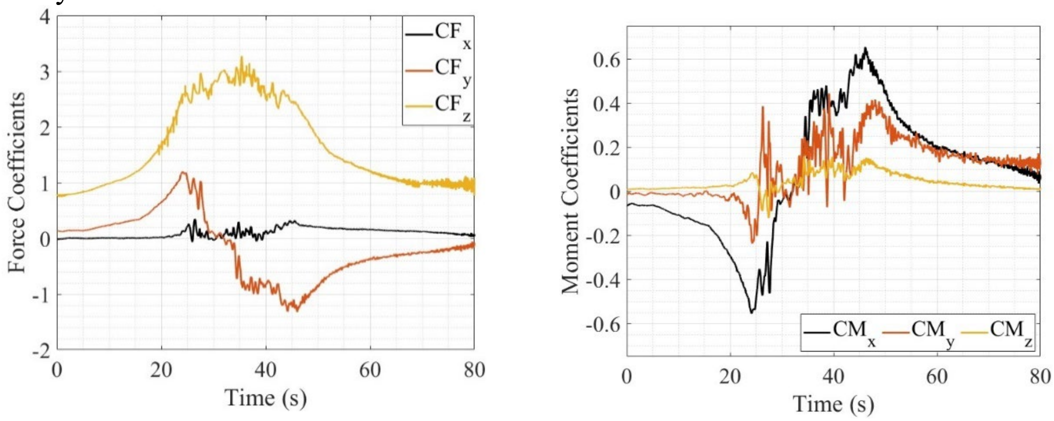

a) b)

Fig. 10 Force/Moment Coefficients on PH induced by tornadic winds (Case 2). a) Force coefficients; b) Moment coefficients.

Figures 11 presents the distributions of pressure, velocity, and streamlines when the PH is at the core radius. In Fig. 11a), it is observed that the stagnation point is nearly at 1/3 of the eave height, lower than in Case 1. After the air passes the PH, a larger turbulent area is formed on the leeward wall side than in Case 1. Unlike Case 1, all the incoming air passes the PH through the roof. As shown in Fig. 11c) and Fig. 11d), the flow pattern on the horizontal plane is similar to the MMH case. However, the velocity magnitude in the most area around the PH are all larger than the values in the MMH case, which is because air is accelerated more significantly in Case 2 than in Case 1 since air has more paths to pass through in Case 1. Accordingly, as shown in Fig. 11e), both the highest and lowest values of negative pressure on the building surface are larger in the PH case. This difference is caused by the existence of the open space under the MMH that allows air to flow through in Case 1, which will not compress the air that much and thus the velocity increase is not much, leading to lower pressure. The lower value in CF_y in Case 1 is because the upstream velocity in front of the windward wall (Wall AB) is not reduced that much due to the fact that air has one more path to flow through (underneath the MMH); The lower value in CF_x in Case 1 is because the incoming air can flow through roof, two sides of the MMH, and underneath the MMH, and thus the acceleration of velocity on the two sides (Wall AD and Wall BC) of the MMH is not that much (streamlines on the two sides of the building are not compressed that much). Then the pressure on Wall AB decreases due to the change of stagnation points and the negative pressure on Wall CD decreases due to the decreased pressure in the leeward direction since the speed of incoming flow decreases.

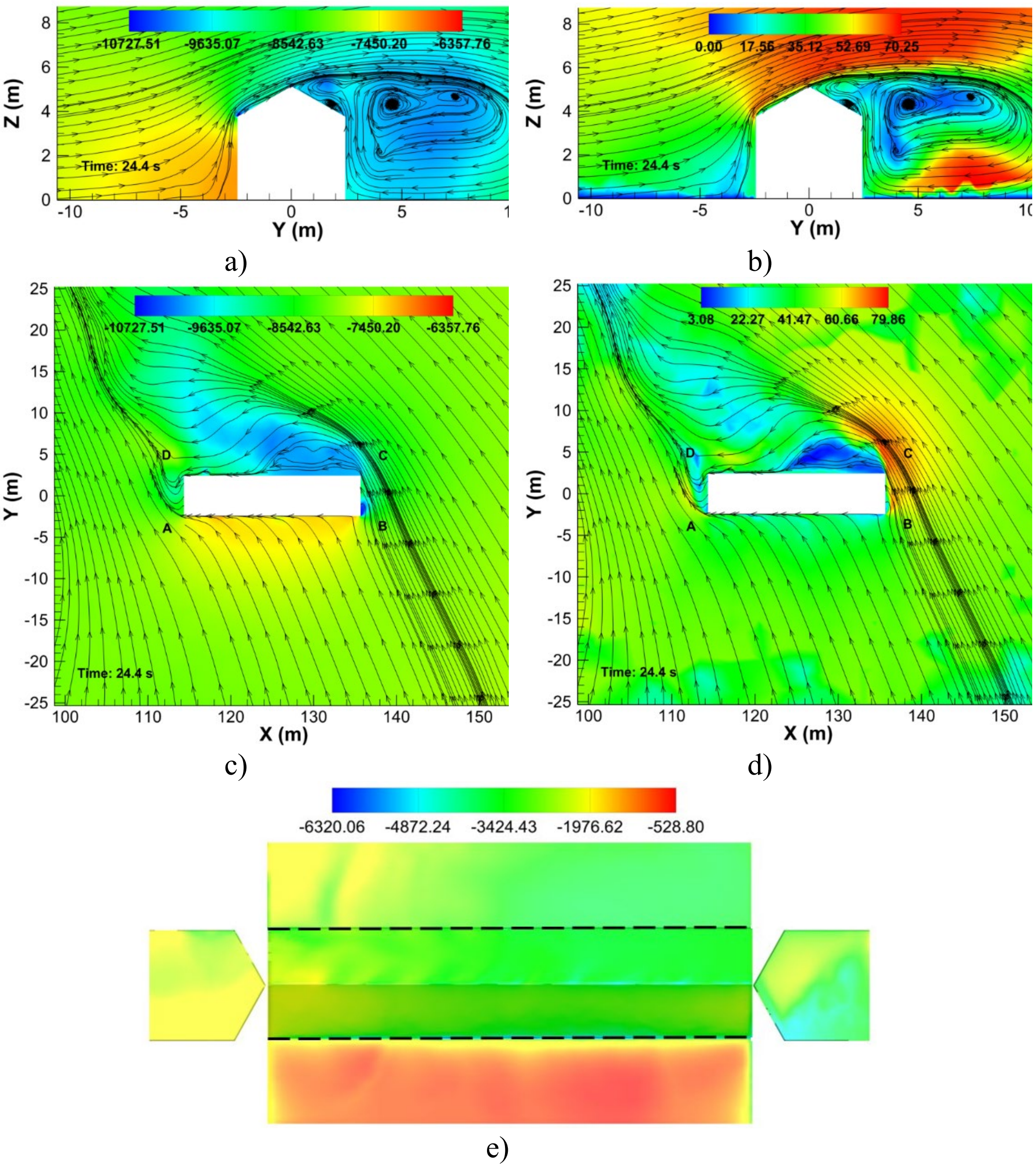

Fig. 11 Contours for pressure, velocity and streamline when the PH is near the core radius: a) Contours for pressure and streamline on the YZ plane through PH; b) Contours for velocity magnitude and streamline on the YZ plane through PH; c) Contours for pressure and streamline on the XY plane through PH at the height of 3 m; d) Contours for velocity magnitude and streamline on the XY plane through PH at the height of 3 m; e) Contours for pressure on PH's surface.

5 Comparison of Wind Effects on MMH Induced by Tornadic Winds and Equivalent Straight-line Winds (between Case 1 and Case 3)

5.1 Simulation Setup for Producing Equivalent Straight-line Wind Field

For comparison, an equivalent straight-line wind field is established. The height, width and length of the flow field are 100m, 400m and 600m, respectively. The center of the MMH is 200 m away from the velocity inlet and 400 m away from the pressure outlet. Large eddy simulation (LES) is applied to obtain the wind effects of straight-line winds on the MMH. The velocity profile applied at the velocity inlet (V) is governed by

$$V = V_r \times (\frac{z}{H_r})^{0.2} \tag{7}$$

where H_r denotes the reference height. In this case, it is 10m, which is the height applied in tornadic wind field to capture the space-averaged velocity. V_r is the velocity at the reference height H_r. In this simulation, $V_r = 54.5\ m/s$, which is the same as the horizontal resultant velocity at the height of 10m in tornadic wind field. The turbulence intensity and integral length scale of turbulence are defined based on Eq. 26.11-7.SI and Eq. 26.11-9.SI in the ASCE 7-22, as shown below.

$$I_{\bar{z}} = c\left(\frac{10}{\bar{z}}\right)^{1/6} \tag{8}$$

$$L_{\bar{z}} = l\left(\frac{\bar{z}}{10}\right)^{\bar{\varepsilon}} \tag{9}$$

where c = 0.3, $\bar{\varepsilon}$ = 1/3, l = 97.54 m are terrain exposure constants according to Table 26.11-1 in ASCE 7-22 (ASCE 7-22), and $\bar{z}$ is the equivalent height of the building defined as 60 percent of the total height but not less than 9.14 m. It is worth noting that the National Weather Service (NWS) has recently implemented issuing wireless emergency alerts (WEAs) to individuals' cell phones for severe thunderstorms (destructive damage threat) with expected winds of at least 80 mph (35.71 m/s). The wind speed in this simulation is much higher than 35.71 m/s and thus would trigger the issuance of WEAs.

5.2 Comparison of Wind Effects Induced by Tornadic Winds and Equivalent Straight-line Winds

The mean force/moment coefficients on the MMH in Case 3 are collected over 60 s, as shown in Table 3. It is found that all the force/moment coefficients in Case 3 are much smaller than those in Case 1. To be exact, CF_y and CM_x in Case 1 are 87% and 88% higher than those in Case 3. These findings indicate that the MMH may not be able to survive from tornados based on the current wind design code, which is based on straight-line winds, although many manufacturing companies state that the MMH is safe to resist hurricane winds. In addition, the force acting on the floor bottom (CF_{z_bot}) is much greater than the force acting on the roof (CF_{z_roof}) in the straight-line wind field. This is because the pressure under straight-line wind field is mainly caused by aerodynamic force, related to the flow pattern modification and accordingly velocity change. To be specific, the air flow under the floor bottom is compressed more severely than that over the roof, leading to higher velocity acceleration under the floor bottom and accordingly lower pressure (larger negative pressure).

Table 3. Mean force coefficients and moment coefficients in Case 3

CF_x	CF_y	CF_z	CF_{z_roof}	CF_{z_bot}	CM_x	CM_y	CM_z
0.0022	0.62	-0.33	0.25	-0.58	-0.32	-0.0039	-0.0009

Figure 12 presents the contours for mean pressure, mean velocity magnitude and streamlines for the MMH in the straight-line field. The mean values are averaged over the collected instantaneous values collected in 60 s during the simulation. Compared to

Case 1, the maximum values of positive pressure and negative pressure in the straight-line field (-3165 Pa and 1864Pa from Fig. 12a)) are much higher than the respective values in the tornadic wind field (-10421 Pa and -6357 Pa). This is due to the different flow nature of tornadic wind field and straight-line wind field. For the tornadic wind field, partial air through open space under MMH goes up near the leeward wall due to the vertical velocity components. Since the straight-line wind does not have the vertical velocity as in the straight-line wind field, the air keeps flowing horizontally after passing the open space. This results in the low wind speed in the vortex shedding area (negative pressure presents) and this area is much larger than that in the tornadic wind field. On the horizontal plane, vortex shedding mainly occurs at Corner A and Corner B, and also occurs behind Wall CD. In addition, the wind flow is symmetric, which results in CF_x to be close to zero. The pressure on the MMH's surface in the straight-line wind field is similar to the distribution in the tornadic wind field but the magnitude is smaller. The similar distribution is because in the tornadic wind field the flow at core radius presents nearly symmetric pattern in the horizontal direction due to the large radius of curvature, which is closed to the straight-line wind field.

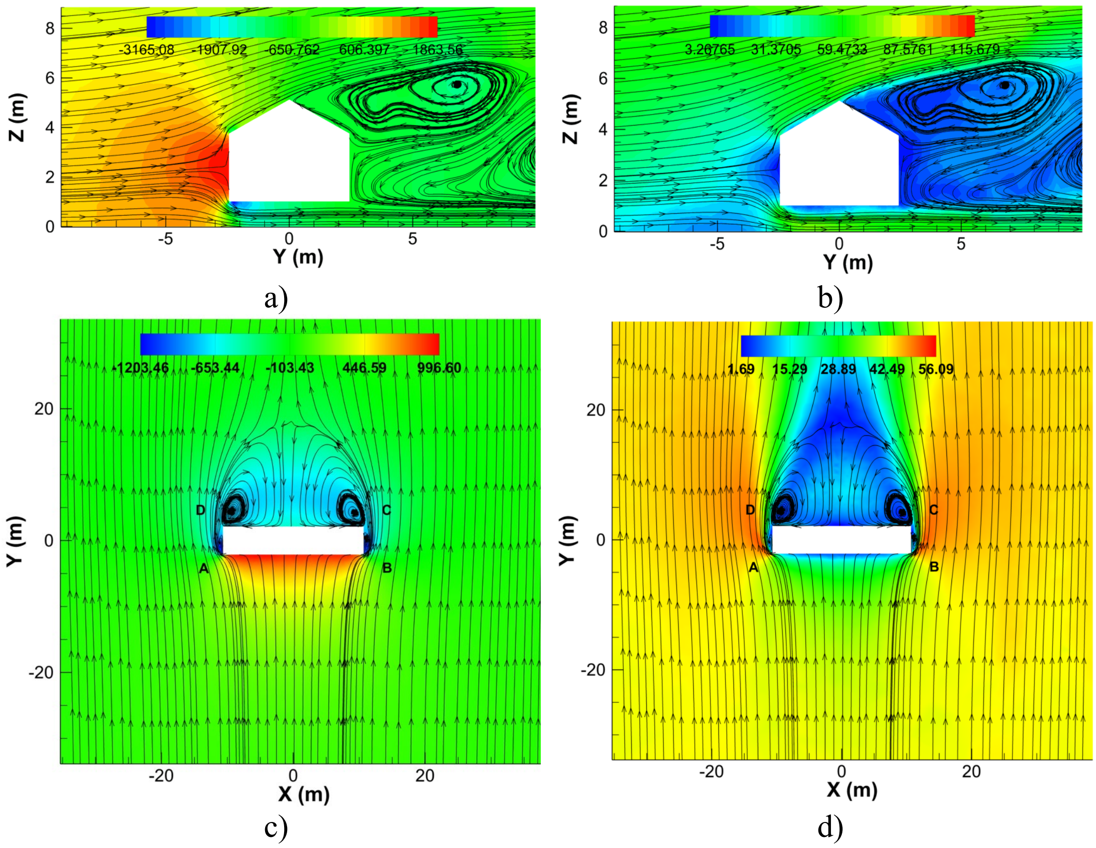

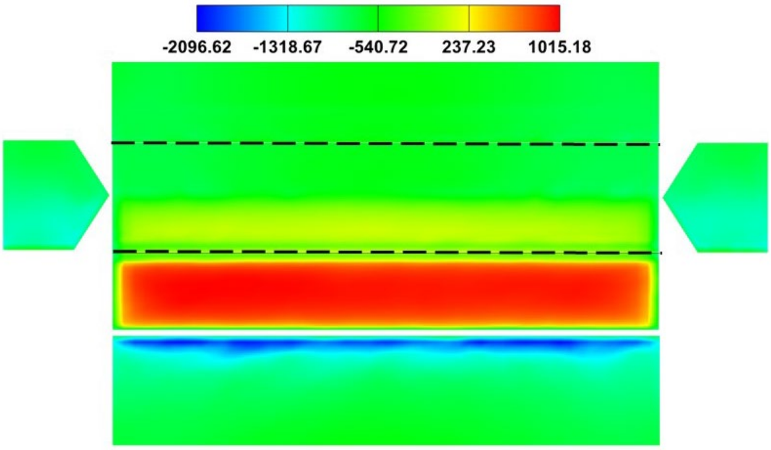

e)

Fig. 12 Contours for mean pressure, mean velocity and streamline when the MMH is in the straight-line wind field: a) Contours for pressure and streamline on the YZ plane through MMH; b) Contours for velocity magnitude and streamline on the YZ plane through MMH; c) Contours for pressure and streamline on the XY plane through MMH at the height of 3 m; d) Contours for velocity magnitude and streamline on the XY plane through MMH at the height of 3 m; e) Contours for pressure on MMH's surface.

6. Conclusions

In this paper, the wind effects induced by a tornado on an MMH is investigated using CFD simulation and reveal (1) the difference in tornadic wind effects between an MMH and its associated PH (home with classical on-site construction), and (2) the difference in wind effects between tornadic winds and the equivalent straight-line winds. After comparing force coefficients, moment coefficients, pressure contours and velocity contours and streamline in each case, the following conclusions are drawn.

1. **Characterizing the forces on an MMH under tornadic winds.** When tornadic winds pass an MMH, the forces in the horizontal directions (F_x and F_y) are greater than the total force in the vertical direction (F_z). Although the total force along the vertical direction acting on the entire MMH seems small, the uplift force acting on the roof and the downward force acting on the floor bottom are significant, much greater than F_x and F_y. They can cause damage to the roof and floor bottom; they can apply significant tensile forces on the joints/connection.
2. **Comparing the tornado-induced forces/pressure on an MMH and PH.** Compared to a PH with the same geometry under tornadic winds, the total force along horizontal direction acting on an MMH is smaller than that for a PH under the same tornadic winds, because of the existence of open space under MMH make the flow smoother; peak pressure on an MMH under tornadic winds is also smaller, because of the higher wind speed around PH.
3. **Comparing the forces on an MMH between straight-line winds and tornadic winds.** Compared to an MMH under straight-line winds, the forces acting on the roof and floor bottom along the vertical direction under tornadic winds are much larger, as the pressure on MMH's surface is caused by both high wind speed and low negative pressure due to atmospheric pressure drop. In addition, the total force along horizontal direction is also larger for an MMH under the tornadic winds. Related to design wind load for MMH, a factor may be introduced to compensate the underestimated wind load caused by tornadoes.

In the future, the obtained findings on MMH in both tornado and straight-line fields will be used to modify the current wind design for MMHs and to design the in-ground anchoring system for MMHs. Also, parametric studies will be conducted to investigate the influence of building orientation on the wind loading induced by tornadoes.

Data availability

Some or all data, models, or code generated or used during the study are available from the corresponding author by request.

1. Numerical tornado models in ANSYS FLUENT
2. Data post-processing MATLAB code

Acknowledgement

The authors greatly appreciate the financial support from the VORTEX-SE Program within the NOAA/OAR Office of Weather and Air Quality under Grant No. NA20OAR4590452. The authors also greatly appreciate the financial support from National Science Foundation, through the project, "Damage and Instability Detection of Civil Large-scale Space Structures under Operational and Multi-hazard Environments" (Award No.: 1455709), and two other projects (#1940192 and #2044013).

References

Anderson, W. K., & Bonhaus, D. L. (1994). An implicit upwind algorithm for computing turbulent flows on unstructured grids. *Computers & Fluids*, *23*(1), 1-21.

Ansys® Academic Research Fluent, Release 19.1

American Society of Civil Engineers. (1994, February). Minimum design loads for buildings and other structures. American Society of Civil Engineers.

American Society of Civil Engineers. (2022, January). Minimum Design Loads and Associated Criteria for Buildings and Other Structures. American Society of Civil Engineers.

Barth, T., & Jespersen, D. (1989, January). The design and application of upwind schemes on unstructured meshes. In *27th Aerospace sciences meeting* (p. 366).

FEMA, 2012: *Spring 2011 tornadoes: April 25–28 and May 22, Building performance observations, recommendations, and technical guidance*. Mitigation Assessment Team Report, FEMA P-908, 512 pp. [Available online at http://www.fema.gov/library/viewRecord.do?.]

Haan Jr, F. L., Balaramudu, V. K., & Sarkar, P. P. (2010). Tornado-induced wind loads on a low-rise building. *Journal of structural engineering*, *136*(1), 106-116.

Hangan, H., & Kim, J. D. (2008). Swirl ratio effects on tornado vortices in relation to the Fujita scale. *Wind & structures*, *11*(4), 291-302.

Hu, H., Yang, Z., Sarkar, P., & Haan, F. (2011). Characterization of the wind loads and flow fields around a gable-roof building model in tornado-like winds. *Experiments in fluids*, *51*(3), 835-851.

Ishihara, T., Oh, S., & Tokuyama, Y. (2011). Numerical study on flow fields of tornado-like vortices using the LES turbulence model. *Journal of Wind Engineering and Industrial Aerodynamics*, *99*(4), 239-248.

Kis, A. K., & Straka, J. M. (2010). Nocturnal tornado climatology. *Weather and Forecasting*, *25*(2), 545-561.

Kosiba, K., & Wurman, J. (2010). The three-dimensional axisymmetric wind field structure of the Spencer, South Dakota, 1998 tornado. *Journal of the Atmospheric Sciences*, *67*(9), 3074-3083.

LaDue, D. S. (2019). Experiences and Practices with Public Tornado Sheltering in Alabama. Pre-Summit Workshop on Public Tornado Shelters: Opportunities and Challenges for Improving Tornado Safety, *National Tornado Summit & Disaster Symposium*, Oklahoma City, Oklahoma, Oklahoma Insurance Department.

Leonard, B. P. (1991). The ULTIMATE conservative difference scheme applied to unsteady one-dimensional advection. *Computer methods in applied mechanics and engineering*, *88*(1), 17-74.

Liu, Z., Zhang, C., & Ishihara, T. (2018). Numerical study of the wind loads on a cooling tower by a stationary tornado-like vortex through LES. *Journal of Fluids and Structures*, *81*, 656-672.

Lott, N., A. Smith, T. Houston, K. Shein, and J. Crouch, 2012: Billion dollar US weather/climate disasters, 1980-2011. National Climatic Data Center. [Available online at http://www.ncdc.noaa.gov/oa/reports/billionz.html.]

Mishra, A. R., James, D. L., & Letchford, C. W. (2008). Physical simulation of a single-celled tornado-like vortex, Part A: Flow field characterization. *Journal of Wind Engineering and Industrial Aerodynamics*, *96*(8-9), 1243-1257.

Natarajan, D., & Hangan, H. (2012). Large eddy simulations of translation and surface roughness effects on tornado-like vortices. *Journal of Wind Engineering and Industrial Aerodynamics*, *104*, 577-584.

National Institute of Standards and Technology (NIST), 2014: Technical Investigation of the May 22, 2011, Tornado in Joplin, Missouri, 428 pp., DOI: http://dx.doi.org/10.6028/NIST.NCSTAR.3

National Weather Service (NWS), 2018: Tornado Awareness. National Oceanic and Atmospheric Administration. [Available online at https://weather.gov/cae/tornado.html.]

National Weather Service (NWS), 2019: Annual U.S. Killer Tornado Statistics. [Available online at https://www.spc.noaa.gov/climo/torn/fatalmap.php.]

Nicoud, F., & Ducros, F. (1999). Subgrid-scale stress modeling based on the square of the velocity gradient tensor. *Flow, turbulence and Combustion*, *62*(3), 183-200.

NOAA (2023). January 21 – 22, 2017 Tornado Outbreak. NOAA, accessed on June 30, 2023, https://www.weather.gov/ffc/20170121_22_tornadoes.

Razavi, A., & Sarkar, P. P. (2018). Tornado-induced wind loads on a low-rise building: Influence of swirl ratio, translation speed and building parameters. *Engineering Structures*, *167*, 1-12.

Refan, M. (2014). Physical simulation of tornado-like vortices. Dissertation, The University of Western Ontario, 174 pp.

Roueche, D.B. et al. (2019) "StEER - 3 March 2019 Tornadoes in the Southeastern US: Field Assessment Structural Team (FAST) Early Access Reconnaissance Report (EARR)." DesignSafe-CI.

Sabareesh, G. R., Matsui, M., & Tamura, Y. (2012). Dependence of surface pressures on a cubic building in tornado like flow on building location and ground roughness. *Journal of wind engineering and industrial aerodynamics*, *103*, 50-59.

Selvam, R. P., & Millett, P. C. (2003). Computer modeling of tornado forces on a cubic building using large eddy simulation. *Journal of the Arkansas Academy of Science*, *57*(1), 140-146.

Sengupta, A., Haan, F. L., Sarkar, P. P., & Balaramudu, V. (2008). Transient loads on buildings in microburst and tornado winds. *Journal of Wind Engineering and Industrial Aerodynamics*, *96*(10-11), 2173-2187.

Strader, S. M., & Ashley, W. S. (2018). Finescale assessment of mobile home tornado vulnerability in the central and southeast United States. *Weather, climate, and society*, *10*(4), 797-812.

Strader, S. M., Ash, K., Wagner, E., & Sherrod, C. (2019). Mobile home resident evacuation vulnerability and emergency medical service access during tornado events in the southeast United States. *International journal of disaster risk reduction*, *38*, 101210.

Sutter, D., & Simmons, K. M. (2010). Tornado fatalities and mobile homes in the United States. *Natural Hazards*, *53*(1), 125-137.

U.S. Census Bureau, 2019: American Community Survey Data Profiles. [Available online at https://www .census.gov/acs/www/data/data-tables-and-tools/data-profiles/]

Van Doormaal, J. P., & Raithby, G. D. (1984). Enhancements of the SIMPLE method for predicting incompressible fluid flows. *Numerical heat transfer*, *7*(2), 147-163.

Wurman, J., & Alexander, C. R. (2005). The 30 May 1998 Spencer, South Dakota, storm. Part II: Comparison of observed damage and radar-derived winds in the tornadoes. *Monthly weather review*, *133*(1), 97-119.

Zhao, Y., Yan, G., & Feng, R. (2021). Wind flow characteristics of multivortex tornadoes. *Natural Hazards Review*, *22*(3), 04021015.